Network based estimation of wind farm power and velocity data under changing wind direction

Genevieve M. Starke¹, Paul Stanfel³, Charles Meneveau¹, Dennice F. Gayme¹, and Jennifer King²

Abstract—This paper describes an estimation algorithm for velocity and power output signals in a wind farm under changing wind direction. A graph-theoretic definition describes the wind farm as a collection of nodes (turbines) and time-varying weighted edges (inter-turbine wake propagation) that change as a function of incoming wind direction. The velocity at each turbine is determined through a discrete input-output model. Changes in wind direction serve as the input and the output is defined in terms of a time-varying weighted adjacency matrix that depends on the time-delay of information propagation between turbines. These delays, which are defined in terms of the advection speed of the wind and the distance between the turbines, capture the delayed effect of wind direction changes on the inter-connectivity of the graph as the wind conditions at the farm inlet propagate through the turbine array. An eventbased update framework is employed to capture time-dependent topology changes due to shifts in wind direction. Simulation results for dynamically changing wind inlet directions to a circular wind farm are compared to predictions from both the static and dynamic versions of the FLOw Redirection and Induction in Steady State (FLORIS) model. The approach is shown to enable real-time tracking of dynamic changes to wind farm power output within a framework that can be easily integrated into real-time, horizon-based, control strategies that typically do not account for wind direction changes.

I. INTRODUCTION

Analytical wake models have long been used to predict the velocity deficits of individual turbines, see e.g. [1], [2], [3]. Recent work has made significant strides in refining these models in combination with a variety of wake superposition approaches to generate accurate estimates of the total farm power output over a range of turbine layouts for fixed wind directions, see e.g. [4], [5], [6], [7]. Changes in total wind farm power output for different wind directions have also been characterized in terms of fixed wind inlet angles to a given wind farm [8]. Few studies address the dynamic behavior of the farm as the wind direction changes. However, accounting for the effect of these changes has been shown to improve power output estimates [9] and produce more effective wake steering control versus approaches that assumed a static wind direction [10], [11].

Prevailing methods typically account for small changes in wind direction as an uncertainty that is included in simulations or models by taking a weighted average of the results over a range of wind inlet angles surrounding a desired value. Prior work has demonstrated that averaging the results of Reynolds-averaged Navier-Stokes (RANS) wind farm simulations in this manner improves predictions of the velocity deficit [12]. This approach also improves the agreement between wake model power output predictions and field data [13].

Taking the further step of accounting for dynamically changing wind direction or sweeps over a range of wind directions is challenging and computationally intensive. Previous approaches include incorporating the directional changes within a high-fidelity precursor simulation that then generates inflow conditions for a second large-eddy simulation (LES) of the wind farm [9], [14] as well as simulations with a dynamically changing reference frame [15]. Other work employs a nested simulation framework, where weather phenomena are modeled in the larger domains, and the wind farm is located in the smallest domain [16]. These detailed studies have provided a greater understanding of the phenomena and highlighted the difficulties of modeling the associated dynamic changes in wind farm power. For example, the LES of Munters et al. [9] show that a wind farm can experience a sharper drop in power output during a dynamic wind direction sweep than would be predicted through a series of static simulations at each different but constant wind inlet direction. This unforeseen reduction in power output can have a number of impacts in terms of forecasting the power available from the wind farm for the power grid. Control approaches require capturing these dynamic effects in real-time, which limits the applicability of the computationally expensive prior approaches based on LES or nested models.

This work takes steps towards a control-oriented modeling approach through the development of an estimation algorithm that leverages a network framework to compute the time evolution of the wind speed at the turbine hub-height and corresponding power output throughout the wind farm under dynamically changing wind inlet directions. Our approach exploits prior work showing the promise of representing a wind farm as a network of turbines described by a directed graph with the turbines as nodes and the interactions between turbines (i.e., the inter-turbine wake propagation) as edges, see e.g. [17], [18]. Those authors showed that the combination of such a model with a consensus algorithm led to improved wind farm speed estimates given noisy field data. The performance of optimal control algorithms has also been improved by adding constraints based on the corresponding wind farm graph [19]. A related network model in [20] used

¹ Genevieve M. Starke, Charles Meneveau and Dennice F. Gayme are with the Department of Mechanical Engineering, Johns Hopkins University, Baltimore, Maryland 21218, USA; email: gstarke1@jhu.edu, meneveau@jhu.edu, dennice@jhu.edu

³ Paul Stanfel is affiliated with Colorado School of Mines; email: pstanfel@alumni.mines.edu.

² Jennifer King is with the National Renewable Energy Laboratory; email: Jennifer.King@nrel.gov.

correlations between power output data from turbines to form real-time graphs describing the interactions between turbines in the wind farm. Graph representations have also been used to study the arbitrage potential of kinetic energy stored in aligned wind farm configurations [21].

These previous studies relied on static graphs that are not designed to account for the dynamic changes in the turbine interconnections resulting from real-time changes in the wind inlet direction. Accounting for these dynamics is complicated by the fact that changes in the wind direction propagate downstream at different rates depending on the inlet velocity and the geometry of farms. Therefore changes at the inlet may not be seen at the outlet until several time steps later. We account for these behaviors by introducing a time-varying graph framework with edge switching [22]. This type of graph model has been widely used to capture similar types of information propagation structures, such as transportation networks [23], [24], [25]. We adopt this model to our problem setting by defining edges in terms of the time delays associated with the turbine to turbine propagation of changes in wind inlet direction as these effects travel through the farm. This behavior is captured using a time-dependent adjacency matrix that depends on the individual time delays associated with each edge. We impose the dynamic changes in the graph structure due to shifting wind direction through an event-based framework. Our algorithm is then constructed as an input-output map that outputs predictions of the transient response of the system to a change in wind direction. Each step in the algorithm is computationally efficient enough to be implemented in realtime, horizon-based, control strategies, which is an advantage over current methods that are able to account for dynamic wind direction changes.

The rest of the paper is organized in the following way: The model is described in detail in Section II. The model is validated using steady-state results from an LES and compared with a dynamic FLORIS simulation of a changing wind direction in Section III. Section IV presents conclusions and discusses directions for future work.

II. MODEL FRAMEWORK

We represent the wind farm as a directed graph $\mathscr{G} =$ $(\mathcal{N}, \mathcal{E})$, where the turbines define the nodes \mathcal{N} and the edges $\mathscr E$ describe the directed interconnections between turbines. In particular, when the wake of turbine *j* influences turbine i, there is a directed edge connecting node j to node i with non-negative edge weight whose magnitude is defined by the strength of the interaction. The adjacency matrix of \mathscr{G} , denoted by Λ , therefore has elements $\lambda_{i,j} = 1$ if Turbine *i* is in the wake of Turbine *j* and $\lambda_{i,j} = 0$ if Turbine *i* is not in the wake of Turbine j. We designate turbines not affected by the wakes of other turbines as freestream turbines, and these turbines act as the head nodes of the graph. Clearly, the structure of the wind farm means that the graph will not always, or perhaps ever, be connected. However, we can separate the graph into connected subgraphs, composed of leader-follower trees. The lead turbines are the freestream turbines, and the follower turbines for each subgraph are all the turbines that are weakly connected to each leader turbine, i.e. there exists a directed path from the lead turbine to each follower. In this way, we can stack multiple connected subgraphs to obtain a representation of the entire system.

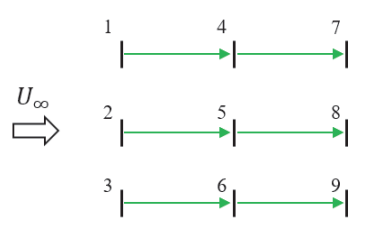


Fig. 1. Example of a graph for an aligned wind farm.

Figure 1 shows an example of a graph for an aligned wind farm where, based on the freestream velocity U_{∞} , nodes 1, 2, and 3 correspond to freestream turbines, i.e., the turbines not affected by wakes of other turbines. For the given wind direction the graph structure is comprised of three line graphs with the directed edges shown, where the lead turbine of each graph only affects those directly behind it. For example, in Figure 1, for the lead turbine, Turbine 1, the follower turbines would be Turbine 4 and Turbine 7. The three graphs obtained in this example are a product of the wind direction, the wind farm geometry, and the atmospheric conditions. For example, different atmospheric conditions could cause interconnections between the three graphs if, e.g., increased prevailing turbulence levels cause larger wake expansion coefficients leading to lateral wake overlaps. Changes in these conditions may also result in leader-follower trees that have shared nodes which must be taken into account in the implementation of the model. The next three subsections describe the building blocks of the input-output estimation algorithm.

A. Wind Farm System Graph Identification

We now describe how to identify the steady state graph representation of the wind farm corresponding to a given wind direction. The graph of the wind farm depends on the geometry and the current atmospheric conditions. Voronoi tessellation is used to partition the domain into cells obtained by placing each vertex equidistant from three nodes (turbines). We determine the freestream turbines by drawing a vector from each turbine location to the front of the farm along the current wind inlet direction. If the line only crosses one cell, its own, to reach the front of the farm, then it is determined to be a freestream turbine. Figure 2(a) shows an example of the line drawn to the front of the farm from the ninth turbine.

The turbines that are not identified as freestream for a given wind direction are then tested to determine if they are in the wake of another turbine. The wake of each turbine is defined through a linear wake expansion with expansion coefficient k_w determined from the atmospheric conditions

$$k_w = \alpha^* \frac{u^*}{U_\infty}.$$
(1)

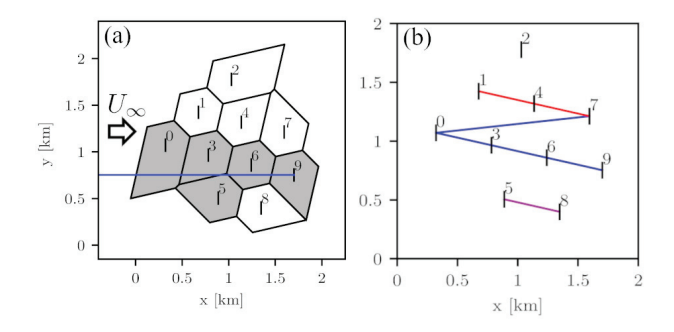


Fig. 2. A simple 10 turbine wind farm example illustrating the process of defining the wind farm graph. (a) Voronoi cells drawn for a left-to-right wind direction. The grey shaded cells are the cells on the line from the ninth node (turbine) to the front of the farm. (b) The leader-follower graphs resulting from applying the algorithm to this wind farm with left-to-right wind direction. The different colors represent subgraphs with independent lead turbines.

Here u^* is the friction velocity, U_{∞} is the freestream velocity, and α^* is a model flow parameter of order one. A turbine is said to be in the wake of an upstream turbine if a line with slope k_w (in the coordinate frame of the incoming wind direction) extending from either edge of the upstream turbine hits the given turbine. To streamline the process, for each non-freestream turbine, we only test the cells that the line drawn to identify freestream turbines crossed to reach the front of the farm for that particular turbine. Taking the example in Figure 2(a), the cells of the turbines that would be tested for Turbine (node) 9 are shaded gray. If the upstream turbine's wake affects the current turbine, there is an edge defined between these turbines (nodes). The graph formed using the configuration shown in Figure 2(a) and $k_w = 0.0625$ is shown in Figure 2(b), where there is a subgraph associated with each of the freestream (lead) turbines (nodes 0, 1, 2, and 5) and the different subgraphs are represented by different colors. In this case Turbine 9 is not in the wake of Turbine 5, even though the cell surrounding that turbine is shaded (i.e. the line crosses through it). However, a larger value of k_w may lead to a connection between these turbines. Further discussion of the definition of the wake coefficients for each turbine is provided in the next subsection.

Having described the process for identifying the system graph, we next specify the system dynamics.

B. System Dynamics

The states of the system are the velocity deficits resulting from the interactions between each turbine pair (i.e. the edges of the graph). To define this quantity we use the concept of 'deficit coefficients', which represent the normalized velocity deficits between each turbine pair, see e.g. [26]. Our description of the deficit coefficient at Turbine i caused by Turbine j, represented by ϕ_i^j , is adapted from an existing turbine deficit model [6] that uses a super Gaussian wake profile. In particular, we apply this model in the far wake limit, which produces a fully Gaussian wake profile and leads

to the following definition of the deficit coefficient

$$\phi_i^j = a \left(\frac{1}{1 + 2k_w \Delta d_i^j} \right)^2 \left[1 + \operatorname{erf} \left(\sqrt{2} \Delta d_i^j \right) \right] W_i^j, \quad (2)$$

where a is the induction factor of the turbine, which is related to the local coefficient of thrust (C'_T) by $a = C'_T/(4+C'_T)$. The direct downstream distance between turbines j and i normalized by the diameter of the turbines is Δd_i^j . The variable W_i^j is the average of the linear superposition wake function (Eq. 10 in Ref. [6]) for the wake of Turbine j over the disk area of Turbine i, which represents the extent of the effect of the wake of Turbine j. This coefficient can be computed as

$$W_i^j = \frac{1}{2\pi R_i^2} \int_0^{R_i} \int_0^{2\pi} W(D\Delta d_i^j, r_{i,j}) \ r_i \ d\theta dr_i, \tag{3}$$

where the variable $r_{i,j}$, which denotes the distance from the center of Turbine j's wake to an infinitesimal point on the disk area Turbine i, is found using $r_{i,j} = \sqrt{(R_j + r_i \cos \theta)^2 + (r_i \sin \theta)^2}$. Here, R_j is the distance between the center of the wake from Turbine j and the center of the disk of Turbine i.

The wake expansion coefficient varies throughout the farm depending on the properties of the farm. The local wake coefficient values for Turbine i, denoted by k_{w_i} , lie within an interval bounded by a freestream value (k_0) , and a fully developed, or waked, value (k_{waked}) . We define the 'waked' region of the wind farm using the height of the internal boundary layer resulting from the presence of the wind farm in the atmospheric boundary layer [27], [28], [29]. The fully developed 'waked' region begins when the height of the internal boundary layer reaches the maximum boundary layer height, represented by H. Defining the start of the boundary layer as the location of the freestream turbines, we vary the wake expansion coefficient linearly between the two values according to the weighting function

$$k_{w_i} = k_0 + \left(\frac{\delta_i - \delta_0}{H - \delta_0}\right) \left[k_{waked} - k_0\right],\tag{4}$$

where δ_0 represents the initial boundary layer height, and δ_i is the height of the internal boundary layer at Turbine i, modeled according to Eq. 34 of Ref. [6].

To form the state vector Φ_k , the individual deficit coefficients calculated between each turbine pair are stacked in the form

$$\Phi_k = \begin{bmatrix} \phi_1^1 & \phi_1^2 & \phi_1^3 & \dots & \phi_1^N & \phi_2^1 & \dots & \phi_N^{N-1} & \phi_N^N \end{bmatrix}^T.$$
 (5)

Since we model the interactions between each turbine pair individually, the system has N^2 states, where N is the number of turbines. We use the following update model for the dynamics of the state vector

$$\Phi_{k+1} = A \ \Phi_k + E_k, \tag{6}$$

where in this case A = I. The input E_k represents the changes in system state due to the wind direction changes (events) in our framework. The precise form of E_k is detailed in II-C.

The output of the system is the total wake deficit coefficient α , which represents the superposition of the individual deficits that affect a given turbine. Due to the physical system of the wind farm, the current output of the system is a function of the states at earlier times, which depends on edge-specific time delays that arise because of the finite time it takes information to travel between turbines. This information, which comprises quantities such as changes in wind direction or in the wake of a forward turbine, is contained in the flow field, and thus travels at the speed of the flow. In other words, this information is a function of the velocity of the flow field and the distance between two turbines. The time delay associated with information travel from Turbine j to i can be approximated as

$$\tau_{k,(i)}^i = \frac{D \ \Delta d_i^j}{u_i},\tag{7}$$

where u_j is the local velocity at Turbine j, representing the speed that information will propagate to Turbine i. The diagonal of the matrix τ_k will be zeros since there is no delay of information when moving from a turbine to itself. The corresponding output equation is given by

$$\alpha_{k+1} = \Lambda(\tau_k)\Phi_k(\tau_k), \tag{8}$$

where $\Lambda(\tau_k)$ is a time-dependent adjacency matrix and is found from the subgraphs present at the delayed time. The quantity $\Phi_k(\tau_k)$ represents the states of the system as a function of the time delays, and describes the delay of information propagation (here the change in wind direction) through the system. The states are updated at every time step, but the effect of that update does not reach the output until after the time delay. The architecture of this formulation results in a linear superposition of the wake velocity deficit coefficients. These coefficients are related to the velocity deficit through $\delta u_i = \alpha_i U_{\infty}$, which enables the disk velocity of the turbines to be found using

$$U_{d,k+1} = U_{\infty} \left(1 - \alpha_{k+1} \right) \left(1 - \frac{C_T'}{4 + C_T'} \right) \tag{9}$$

where C'_T is the local coefficient of thrust for the turbine.

The power from the wind farm is computed using the disk velocities calculated in Equation (9) as

$$P_k = \frac{1}{2}\rho \left(\frac{1}{4}\pi D^2\right) U_{d,k+1}^3 C_P' \tag{10}$$

where ρ is the air density, $\pi D^2/4$ is the rotor disk area, and C_P' is the local coefficient of power. C_P' is sometimes assumed to be the same as the local coefficient of thrust C_T' (Betz limit), but in applications it is usually less due to losses.

C. Network Changes

Our time-varying graph is based on a log-file approach [22], where the static directions are the snapshots, and the changes between two snapshots - or two wind directions - are cataloged in time. The changes that occur in the graph are then implemented in an event-based framework, wherein

an event is defined when the wind direction changes. The events are then associated with their application times t_k .

For a given event, the model has a current end-goal graph that represents what the final form of the graph will look like after the changes have been applied. When a subsequent event occurs, the final graph for the new wind direction is calculated and compared with the current end-goal graph. Changes between these two graphs are noted and sorted as a function of the time at which the event state reaches a given turbine. This time is computed as the streamwise distance between the turbine and the front of the farm divided by the freestream velocity. Here the front of the farm is defined by the turbine at the front (i.e. the one that first experiences the inlet velocity associated with the new wind direction). Once the changes are defined and sorted, they are integrated into the existing event framework to be applied at the appropriate time in the simulation. The input for the system is then a function of the event parameters that are relevant to the current application time.

$$E_k = f(\Phi_k, \tau_k, \Delta \mathcal{E}_k) \tag{11}$$

Each input is a function of the new state values $\Phi_{e,i}$, the new time delay values $\tau_{e,i}$, and the list of the edge changes $\Delta \mathcal{E}_{e,i}$.

III. RESULTS

A. Simulation Setup

The model is tested using the circular wind, shown in Figure 3, farm comprised of 38 5MW NREL reference turbines [30]. The wind direction is referenced by considering an inflow direction from the north as 0° . It then proceeds in a clockwise direction, which places the standard left-toright inflow to the farm at 270° , as shown in Figure 3. Each turbine has a height $z_h = 90$ meters and a turbine diameter D = 126 meters.

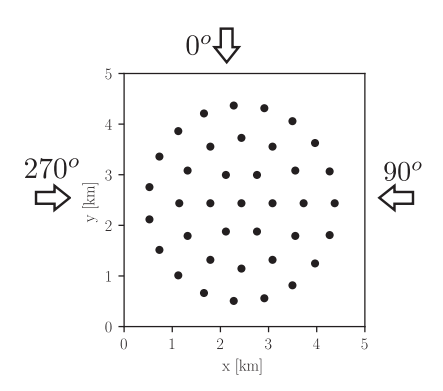


Fig. 3. The circular wind farm configuration used to validate the graph model. The arrows and angles show the orientation of the wind direction.

The model is validated by comparing the steady-state results to the average power from LES using Simulator for Offshore Wind Farm Applications (SOWFA) [31] and the results of several wake models. We focus on comparisons with the Area Localized Coupled (ALC) model, introduced in [29]. The ALC model has been compared to LES of this circular wind farm with good agreement in the power output

over a range of wind directions. Figure 4 reports the output of the ALC model, which was run at intervals of 5° alongside SOWFA data at intervals of 30°. Here it is clear that the ALC model captures trends in the LES power for different static wind directions.

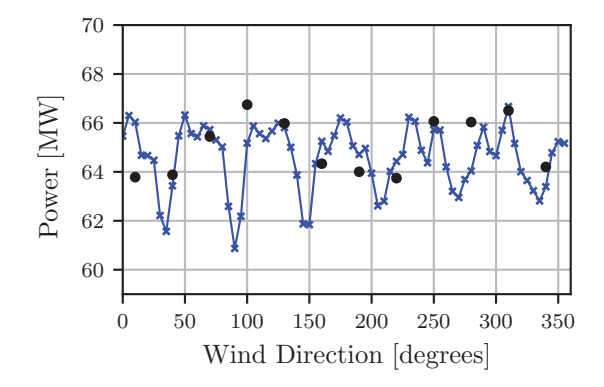


Fig. 4. A plot of the data comparison taken from [29] of the power from the LES data (\bullet) and the results from the ALC model run in 5^o increments (-x-)

The LES have a roughness height of $z_0 = 0.15$ meters and average inflow wind speed of $U_{\infty} = 8.07$ m/s. The simulations use an actuator disk model for the turbines. The wake models use the same turbine parameters and U_{∞} value. The friction velocity for the models is calculated using $u^* = U_{\infty} \ln(z_h/z_{0,lo})$. The values for coefficients of thrust and power are taken from the analysis in [29].

In the graph model, the values of $k_0 = 0.12$ and $k_{waked} = 0.2$ were computed from the average values from runs of the ALC model spanning 90° at 15° increments. The initial boundary layer height δ_0 is computed using a modified top-down model in the atmospheric boundary layer [28]. The maximum boundary layer height was set to 750 m, due to a temperature inversion at that height in the LES.

The dynamic results are compared to modified dynamic FLOw Redirection and Induction in Steady State (FLORIS) simulations under changing inflow directions [32]. FLORIS is a dynamic model where direction changes are also incorporated using time delays. However the outputs of FLORIS are tuned using heuristics, and therefore may not be amenable to real-time control applications. The model was first tested on a direction change from 280° to 270° . The change was implemented at a rate of 2° per minute, for a total time of five minutes. Figure 5(a) shows the power over the wind direction change. The plot also includes a steady-state comparison for an LES simulation, where we only have data for 280° , the Jensen model [1], [2], the coupled model in Shapiro et al. [6], and the ALC model [29].

All the models and LES agree well at 280° except the Jensen model, but the coupled model from Shapiro et al. diverges at 270°. The Jensen model, while lower than the other models, perhaps because the way we define the wake expansion coefficient formulation, exhibits a drop in power from 280° to 270° that is similar in magnitude to that of the graph model, the ALC model, and FLORIS. Since this is the

only model without any optimization of the wake expansion coefficient, the power output numbers may be less due to the the assumption of uniform wake behavior through the farm.

The dynamic response of the graph model in Figure 5(a) is compared to the dynamic FLORIS model implemented with the same direction change, which is represented by the solid line. Both of the models exhibit similar trends, with a ramp down to the 270° value. Though the steady-state FLORIS power for 270° is lower than that of the graph model, both models reach a steady state at very similar times, and the difference in the slope is a result of the variation in the final values. Modeling differences in the wake deficits likely account for the range of values for the power at 270°. The black dashed line in the figure shows what the predicted power would be for the wind farm if the current wind direction was assumed to be valid through the whole wind farm, (i.e. at each wind direction the steady state output power is computed from a static model). In this case, the steady-state prediction would show that all the effects of the change in wind direction are accounted for around the same time that the dynamic direction models start to show the effects of the wind direction change. This illustrates that neglecting the dynamic response to the wind direction change can lead to inaccurate power output predictions.

Figure 5 also shows the graph connections at different points in the wind direction change. The wind direction change is evident in the graph when the initial graph in Figure 5(1) is compared to the final graph in Figure 5(5). In the initial graph, the connections between turbines are predominantly diagonal, while the connections in the final graph reflect the left-to-right inflow direction. The intermediate graphs, in Figure 5(2)-(4), show how the change of direction propagates through the farm.

When considering the wind farm as a graph, the connections do not tell the whole story. We must also consider the intensity of the connections, represented by the weights of the edges. In this context, the weights indicate how much the wake of the leading turbine in the edge affects the power of the following turbine. Figure 6(1)-(5), shows the weighted connections of the graph, where darker colors indicate a stronger connection. We can see the importance of the weights of the connections by noting that even though the graph for the farm with a 280° wind direction appears to have more connections, the connections are relatively weak across the farm. The connections in the graph with a 270° wind direction are much stronger, particularly for the aligned turbines in the center, resulting in a lower overall power.

We also applied the graph model to a longer change in wind direction, starting at 280° and finishing at 250°. The rate of change for the wind direction was kept at 2° per minute, resulting in a total change time of 15 minutes. Figure 7 shows the power in time from the graph model for this change. The steady results agree well with the LES data for the steady state power in both directions, and also with the model from Shapiro et al. [6], the ALC model, and the FLORIS model. The Jensen model is lower than all other points for the 280° case, but is much closer in the 250°

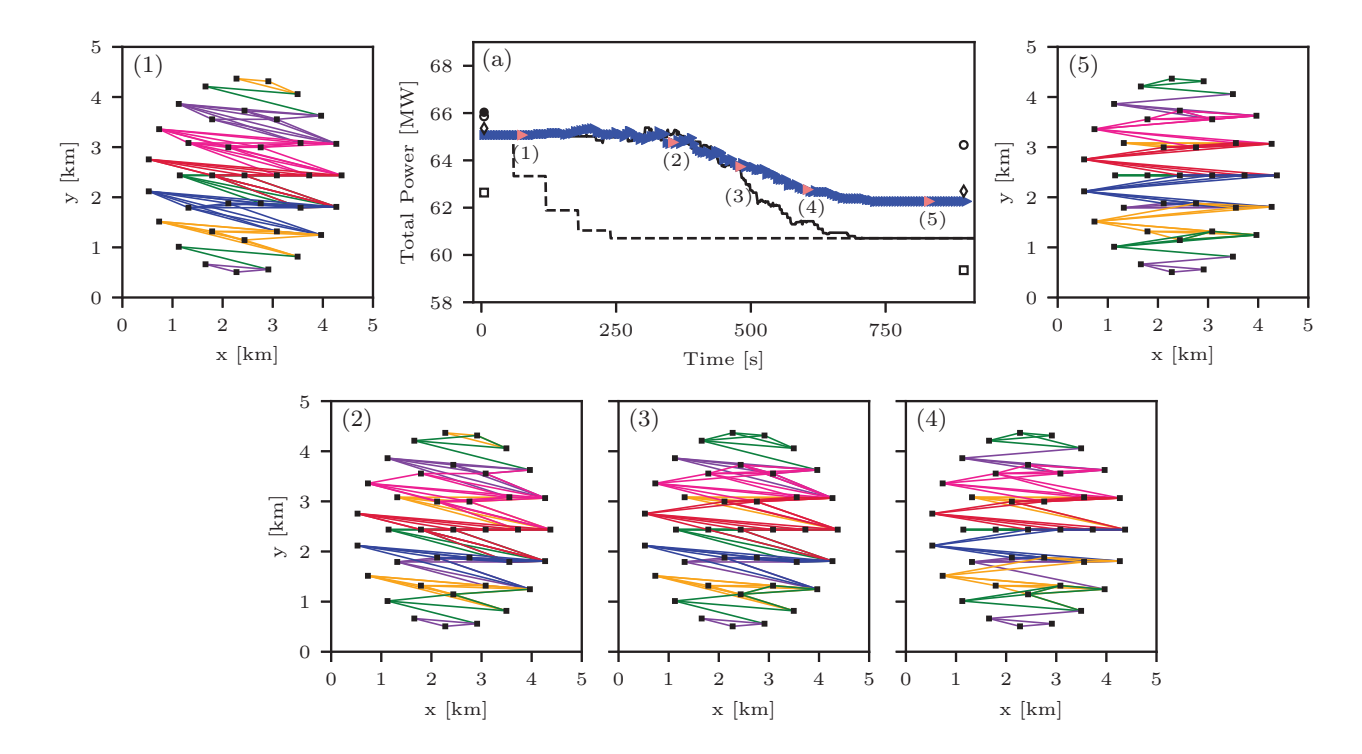


Fig. 5. The central figure (a) shows the power of the graph model (\triangleright) as a function of time as the wind direction changes from 280° to 270°, compared with the dynamic FLORIS simulation (-) and the static power from FLORIS (- -) over the same wind direction change. The model is compared to LES data at 280° (\bullet), the Jensen/Park model (\square), the coupled model from Shapiro et al. [6] (\circ), and the ALC model from Starke et al (\diamondsuit) for both directions. The numbered figures correspond to the connections of the graph of the wind farm at different points in the wind direction change, which are shown by (\triangleright) in (a). Each different color line in Figures (1)-(5) represents a separate subgraph and its connections, each of which have an independent lead turbine.

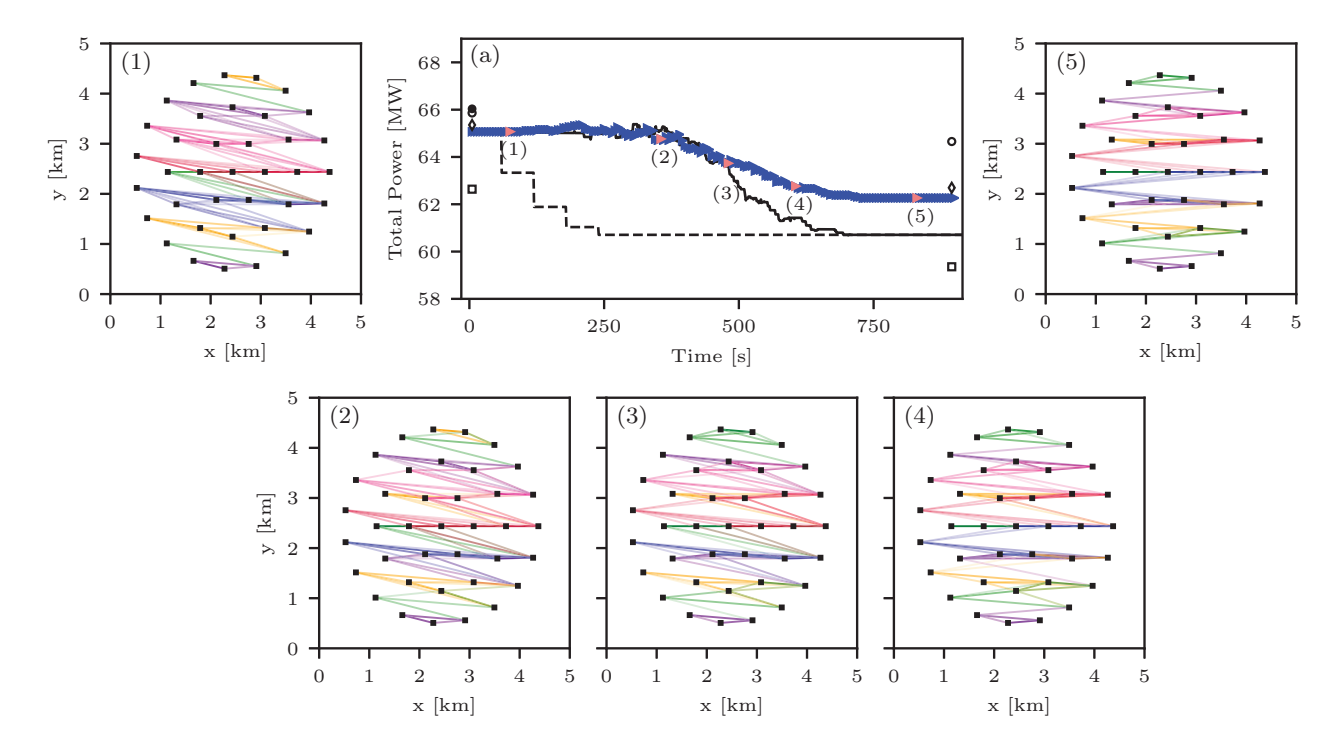


Fig. 6. The central figure (a) shows the power of the graph model (\triangleright) as a function of time as the wind direction changes from 280° to 270°, compared with the dynamic FLORIS simulation (-) and the static power from FLORIS (- -) over the same wind direction change. The model is compared to LES data at 280° (\bullet), the Jensen/Park model (\square), the coupled model from Shapiro et al. [6] (\circ), and the ALC model from Starke et al (\diamondsuit) for both directions. The numbered figures correspond to the weighted connections of the graph of the wind farm, where darker colors indicate stronger connections, at different points in the wind direction change, which are shown by (\triangleright) in (a). Each different color line in Figures (1)-(5) represents a separate subgraph and its connections, each of which have an independent lead turbine.

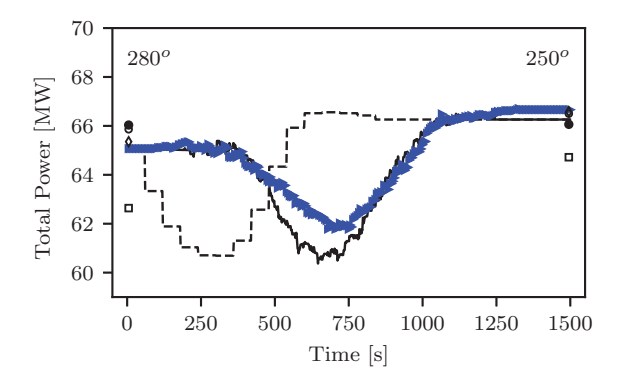


Fig. 7. The power prediction of the graph model (\blacktriangleright) as the wind direction changes from 280^{o} to 250^{o} at a rate of 2^{o} per minute, compared with the FLORIS simulation (-) and the static power from FLORIS (- -) for the same wind directions. The endpoints are compared with LES data (\bullet), the Jensen model (\Box), the model in Shapiro et al.[6] (\circ), and the ALC Model from Starke et al. [29] (\diamondsuit)

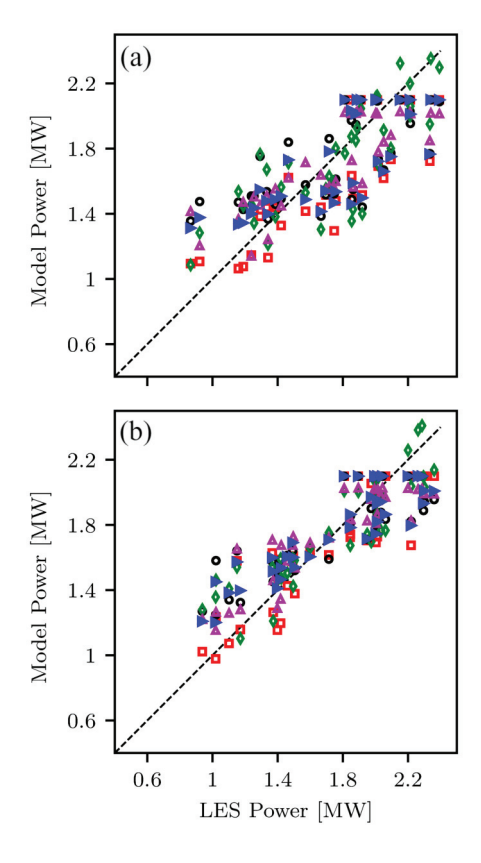


Fig. 8. Scatter plots comparing the model-predicted power with the LES data for the LES wind directions (a) 280^{o} and (b) 250^{o} , for the Jensen model (\square), the model in Shapiro et al.[6] (\circ), the ALC model in Starke et al.[29] (\diamond), the FLORIS model (\blacktriangle), and the graph model (\blacktriangleright). A 1:1 relationship is represented by a 45^{o} line (- -).

case.

In the dynamic response, the graph model is compared with the results from dynamic FLORIS, represented by the solid black line. We can see that the trends of the two models agree well, both exhibiting a dip in power before coming back to a similar value at the end of the simulation. This is a result of the more aligned nature of the farm at 270°, as seen in the previous example. The dynamic responses were again compared with the static step response, depicting the result if the wind direction is changed through the whole farm simultaneously, shown by the black dashed line. While the magnitude and the general trend of these values are similar, the static response reaches the trough and the final wind direction steady state much sooner than the dynamic response. This illustrates that using a static model for wind farm control under a wind direction change would give an inaccurate power prediction, rendering control of the system less effective. For implementation purposes, the graph model is significantly faster than the dynamic FLORIS model, with the entire simulation in Figure 7 taking between two and three minutes. This makes the graph model approximately 20 times faster than the dynamic FLORIS model, which is an important factor for applicability in control applications.

In addition to the average power of the farm, we can compare the individual power for each turbine. Figure 8(a) shows a scatter plot for 280° and Figure 8(b) shows the scatter plot for 250°, where the individual power of the turbines predicted by the Jensen/Park model, the coupled model in [6], the ALC model, the dynamic FLORIS model, and the graph model, are plotted against the average individual turbine power from the LES. The models compare well with the LES power, but with less spread for the 250^{o} direction. Since all the models except the ALC model use a uniform inflow velocity profile, the freestream turbines all give the same value, which can be seen as a horizontal cap on the higher values on both plots, while the ALC model has variation in the freestream turbines. When compared to the wake models, the graph model provides a reasonable prediction of the power for each turbine, and gives an accurate estimation of the total power.

IV. CONCLUSIONS

Operational wind farms are routinely subjected to changing wind inlet conditions that need to be taken into account in algorithms that aim to regulate wind farm power output. This paper introduces a highly efficient analytical wake model applicable to a wind farm under dynamically changing wind directions. The model is an estimation algorithm that enables one to capture propagation of the wind direction changes through the wind farm. The algorithm takes into account the fact that turbines further back in the array do not experience the wind inlet changes until the inlet flow reaches them, which results in a finite time delay. The model was applied to a nonuniform wind farm. The model results are comparable with LES and wake models for a steady wind direction. More importantly, the model captures the behavior of the power output over a wind direction sweep more realistically than

static models, which implicitly assume that the direction of the wind changes for the entire farm simultaneously. The structure and speed of the model lends itself to integration into real-time, horizon-based, control strategies. Future work will examine different wind farm configurations as well as adding wind speed variability and yaw capability to the model. Ongoing efforts include incorporating the model into a power control framework.

ACKNOWLEDGEMENT

G.M.S., C.M. and D.F.G. gratefully acknowledge partial funding support from the National Science Foundation (grant numbers DGE-1746891, CBET-1949778 and CMMI-1635430).

This work was coauthored by the National Renewable Energy Laboratory, operated by Alliance for Sustainable Energy, LLC, for the U.S. Department of Energy (DOE) under Contract No. DE-AC36-08GO28308. Funding provided by the U.S. Department of Energy Office of Energy Efficiency and Renewable Energy Wind Energy Technologies Office. The views expressed in the article do not necessarily represent the views of the DOE or the U.S. Government. The publisher, by accepting the article for publication, acknowledges that the U.S. Government retains a nonexclusive, paidup, irrevocable, worldwide license to publish or reproduce the published form of this work, or allow others to do so, for U.S. Government purposes.

REFERENCES

- N. O. Jensen, "A note on wind generator interaction," Risø National Laboratory, Tech. Rep. Risø-M-2411, 1983.
- [2] I. Katic, J. Højstrup, and N. O. Jensen, "A simple model for cluster efficiency," in *European Wind Energy Assoc. Conf. and Exhibition*, 1986, pp. 407–410.
- [3] M. Bastankhah and F. Porté-Agel, "A new analytical model for windturbine wakes," *Renewable Energy*, vol. 70, pp. 116–123, 2014.
- [4] A. Niayifar and F. Porté-Agel, "A new analytical model for wind farm power prediction," J. Phys.: Conf. Series, vol. 625, p. 012039, 2015.
- [5] R. J. A. M. Stevens, D. F. Gayme, and C. Meneveau, "Coupled wake boundary layer model of wind-farms," *J. Renewable and Sustainable Energy*, vol. 7, no. 2, p. 023115, 2015.
- [6] C. R. Shapiro, G. M. Starke, D. F. Gayme, and C. Meneveau, "A wake modeling paradigm for wind farm design and control," *Energies*, vol. 12, no. 15, p. 2956, Aug 2019.
- [7] H. Zong and F. Porté-Agel, "A momentum-conserving wake superposition method for wind farm power prediction," J. Fluid Mech., vol. 889, p. A8, 2020.
- [8] F. Porté-Agel, Y.-T. Wu, and C.-H. Chen, "A numerical study of the effects of wind direction on turbine wakes and power losses in a large wind farm," *Energies*, vol. 6, no. 10, pp. 5297–5313, 2013.
- [9] W. Munters, C. Meneveau, and J. Meyers, "Turbulent inflow precursor method with time-varying direction for large-eddy simulations and applications to wind farms," *Boundary-Layer Meteorology*, vol. 159, pp. 305–328, 2016.
- [10] A. Rott, B. Doekemeijer, J. Seifert, J. W. Wingerden, and M. Kühn, "Robust active wake control in consideration of wind direction variability and uncertainty," *Wind Energy*, vol. 3, pp. 869–882, Sept 2018.
- [11] E. Simley, P. Fleming, and J. King, "Design and analysis of a wake steering controller with wind direction variability," *Wind Energy Sci.*, vol. 5, no. 2, pp. 451–468, 2020.
- [12] E. G. Antonini, D. A. Romero, and C. H. Amon, "Improving CFD wind farm simulations incorporating wind direction uncertainty," *Re-newable Energy*, vol. 133, pp. 1011 – 1023, 2019.
- [13] M. Gaumond, P.-E. Réthoré, S. Ott, A. Peña, A. Bechmann, and K. S. Hansen, "Evaluation of the wind direction uncertainty and its impact on wake modeling at the Horns Rev offshore wind farm," Wind Energy, vol. 17, no. 8, pp. 1169–1178, 2014.

- [14] T. Chatterjee, N. W. Cherukuru, Y. T. Peet, and R. J. Calhoun, "Large eddy simulation with realistic geophysical inflow of Alpha Ventus wind farm: a comparison with LIDAR field experiments," *J. Phys.:* Conf. Series, vol. 1037, p. 072056, Jun 2018.
- [15] A. Stieren, S. Gadde, and R. J. A. M. Stevens, "Modeling dynamic wind direction changes in large eddy simulations of wind farms," *Renewable Energy*, 2021.
- [16] R. S. Arthur, J. D. Mirocha, N. Marjanovic, B. D. Hirth, J. L. Schroeder, S. Wharton, , and F. K. Chow, "Multi-scale simulation of wind farm performance during a frontal passage," *Atmosphere*, vol. 11, no. 3, 2020.
- [17] J. R. Annoni, C. Bay, K. E. Johnson, E. Dall'Anese, E. W. Quon, T. W. Kemper, and P. A. Fleming, "Wind direction estimation using SCADA data with consensus-based optimization," *Wind Energy Sci.* (Online), vol. 4, no. 2, June 2019.
- [18] J. Annoni, C. Bay, K. Johnson, and P. Fleming, "Short-term forecasting across a network for the autonomous wind farm," in *Proc. of the American Control Conf.*, 2019, pp. 2837–2842.
- [19] J. Annoni, E. Dall'Anese, M. Hong, and C. J. Bay, "Efficient distributed optimization of wind farms using proximal primal-dual algorithms," in *Proc. of the American Control Conf.*, 2019, pp. 4173– 4178
- [20] F. Bernardoni, U. Ciri, M. Rotea, and S. Leonardi, "Real-time identification of clusters of turbines," *J. Phys.: Conf. Series*, vol. 1618, p. 022032, Sep 2020.
- [21] C. R. Shapiro, C. Ji, and D. F. Gayme, "Real-time energy market arbitrage via aerodynamic energy storage in wind farms," in *Proc. of* the American Control Conf., 2020, pp. 4830–4835.
- [22] A. Zaki, M. Attia, D. Hegazy, and S. Amin, "Comprehensive survey on dynamic graph models," *International J. of Advanced Computer* Sci. and Applications, vol. 7, Feb 2016.
- [23] I. Maduako and M. Wachowicz, "A space-time varying graph for modelling places and events in a network," *International J. of Geographical Information Sci.*, vol. 33, no. 10, pp. 1915–1935, 2019.
- [24] F. Xiao and L. Wang, "Asynchronous consensus in continuous-time multi-agent systems with switching topology and time-varying delays," *IEEE Trans. on Automatic Control*, vol. 53, no. 8, pp. 1804–1816, 2008.
- [25] W. Zhu and D. Cheng, "Leader-following consensus of second-order agents with multiple time-varying delays," *Automatica*, vol. 46, no. 12, pp. 1994 – 1999, 2010.
- [26] E. Bitar and P. Seiler, "Coordinated control of a wind turbine array for power maximization," in *Proc. of the American Control Conf.*, June 2013, pp. 2898–2904.
- [27] M. Calaf, C. Meneveau, and J. Meyers, "Large eddy simulation study of fully developed wind-turbine array boundary layers," *Phys. of Fluids*, vol. 22, no. 1, p. 015110, 2010.
- [28] C. Meneveau, "The top-down model of wind farm boundary layers and its applications," J. Turbul., vol. 13, p. N7, 2012.
- [29] G. M. Starke, C. Meneveau, J. R. King, and D. F. Gayme, "The Area Localized Coupled model for analytical mean flow prediction in arbitrary wind farm geometries," *ArXiv preprint*, 2020.
- [30] J. Jonkman, S. Butterfield, W. Musial, and G. Scott, "Definition of a 5-MW reference wind turbine for offshore system development," National Renewable Energy Laboratory, Tech. Rep. NREL/TP-500-38060, 2009.
- [31] M. Churchfield and S. Lee, "NWTC Design Codes (SOWFA)," 2013. [Online]. Available: http://wind.nrel.gov/designcodes/simulator/SOWFA
- [32] NREL, "FLORIS. Version 2.2.3," GitHub repository, 2020. [Online]. Available: https://github.com/NREL/floris